A Self-constraint Model Predictive Control Method via Air Conditioner Clusters for Min-level Generation Following Service

Yunfeng Ma[a,*], Chao Zhang[b], Bangkun Ding[a], Zengqiang Mi[a]

[a]North China Electric Power University, School of Electrical and Engineering, Beinong road, Beijing, 102206, China
[b]University of Manchester, Department of Electrical and Engineering, Oxford road, Manchester, M13 9PL, UK

Abstract

As renewable power generation increases in distribution networks, the real-time power balance is becoming a tough challenge. Unlike simple peak-load shedding or demand turn-down scenarios, generation following requires persistent and precise control due to the temporal response performance of controlled resources. This motivates a comprehensive control design considering the temporal response limitations and execution performance of ACCs when providing such services. Accordingly, this paper proposes a self-constraint MPC that properly allocates the generation following task among different ACCs, consisting of three main parts: response rehearsal, distributed consistency-based power allocation, and real-time task execution. Specifically, the rehearsal knowledge of ACCs is evaluated by introducing model predictive control to track power signals with different values and thus obtain prior factors, including the upward/downward limits and control cost function. On this basis, the coherence of the incremental response costs of different clusters is achieved by containing the prior factors to model the constraints and cost functions. Once the optimised following signals are obtained, a real-time model predictive controller for generation following task execution is employed. Simulations are conducted to verify the feasibility and effectiveness of the proposed method.

Keywords: generation following, air conditioner clusters, ancillary service, response potential, distribution consistency

1. Introduction

The rise in global temperatures poses a significant threat to ecosystems and human well-being[1]. Achieving net-zero targets has become a critical global issue due to the urgency of addressing climate change[2][3]. Besides, geopolitical tensions, like the ongoing Russia-Ukraine war, have introduced uncertainties in the supply of traditional oil and gas resources. This conflict highlights the vulnerability of relying on fossil fuels for energy security. As a result, there is an urgent need to transition to sustainable and renewable energy sources. As reported by the 2023 BP World Energy report[4], the energy transition or electrification becomes an effective way to cope with this problem, such as in the main sections of the power system, transportation, and building. The penetration of onsite renewable power generation may present an unstoppable trend[5]. Under this trend, the variability and uncertainty brought by renewable power may become more evident[6], and the flexibility in the power system needs to be more sufficient.

There have been various techniques[7, 8] developed to address the challenges posed by the variability and uncertainty of renewable power generation. However, one category of technique, the load following service, has not received as much attention. Nonetheless, it has been demonstrated as an effective and cost-efficient approach to managing the hourly net load fluctuations. To the best of the authors knowledge, the earliest definition of "load following service" can be traced back to two articles published in [9] and [10]. The definition of load following is "Load following is the use of online generation equipment to track the intra- and inter-hour changes in customer loads. Unlike the minute-to-minute fluctuations, which are generally uncorrelated among customers, the longer-term changes in customer loads are generally correlated with each other". As highlighted by Ref.[11], the load following service has often been overlooked due to an omission, resulting in a mix-up with the regulation service. This confusion has led to higher

*Corresponding Author
Email address: yf_ma0928@ncepu.edu.cn (Yunfeng Ma)

costs for the California Independent System Operator as they had to purchase the more expensive regulation service when the load following service could have sufficed. Given this scenario, it is economically feasible to separate the load following service from the regulation service. This division allows for a more efficient allocation of resources, with the load following service catering to slow-changing variations and the regulation service addressing fast-changing fluctuations. Some attention has been attracted to the topic of load following service by the market operator in some contries[12],[13]. However, there are still some unsolved issues linked to the competitive provision of LFS[14], including 1) the responsibility of ensuring performance, 2) the number of suppliers, and 3) the payment allocation. Some researchers put their effort into solving some of these problems; the feasibility of procuring load following service through bilateral contracts between the supplier and consumer is verified in [14]. Load following control schemes for generators in electricity bilateral markets are designed in [15] and [16] respectively.

As the proportion of other types of generations increases, such as renewable power generations [17, 18], batteries [19], and nuclear power plants[20, 21] there are also some new attempts to utilise these generations to provide load-following services. The earlier attempt could be traced back to Ref.[17] , where the possible approaches to load following are investigated, and the basic feasibility of load following is demonstrated by simulations. Ref.[18] investigates the method of utilising wind turbines to provide load following service instead of running at the conventional maximum power output. Ref.[19] proposes a dedicated control system for a battery charger in a photovoltaic generator for load-following applications. The above articles prove the feasibility of using renewable power generation to follow load changes. Simultaneously, as the proportion of nuclear power plants (NPP) increases, like more than 75% in France, the NPP are also investigated to run in load following mode, thus balancing the fluctuations in power demand [20]. Furthermore, Ref.[21] gives insights into the economic factors driving NPP to provide flexible power output under the European Energy Roadmap 2050[22]. Besides,there are also some other resources are surveyed to explore the applications for providing load following, such as microturbines[23, 24, 25], fuel cells [26, 27, 28], pressurized water reactors [29], etc.

Most recently, the energy transition has become more unstoppable and urgent than before. The increasing need for electric power incentivizes the utilization of onsite renewable power generation. This trend reminds us that trying to transfer the balancing role from the generation side to the load-side, especially when the distributed energy is deployed more in the distribution network[30, 31, 32], may be a promising solution. On such occasions, utilizing renewable power generation to provide energy supply as much as possible would improve social welfare and seem like an economic way. Very few research are conducted on the topic of load following service by air conditioners [33, 34, 35, 36, 37], Ref.[34] demonstrated the feasibility of tapping the potential of thermostatically controlled loads (TCL) to provide both regulation and load following services. In this discussion part, the simulation results come to the conclusion that the equivalent power storage capacity to provide LFS is 1.25 times that of regulation service, with the same population of TCL. But the performance of the TCLs is not considered. The conclusion motivates us to look deeply into the application of using ACC to follow min-level signals and make full use of the econometrics of ACC, especially with the trend of onsite generation increasing rapidly.

Indeed, the provision of min-level generation following is not like that with simple peak-load shedding or demand turn-down; the generation following service requires a precise control effect and also a relatively longer response time period, usually 1 to 2 hours. There has been some research on the control strategy for air conditioners providing load following service. Ref.[35] evaluated the potential of aggregated heating, ventilating and air-conditioning (HVAC) loads to provide load balancing service, but the control accuracy needs to be significantly improved. Ref.[36] proposed a hierarchical centralized control algorithm of the TCL clusters to provide load following service, but the centralized methods rely highly on communication reliability. Furthermore, a demand response load following distributed pinning control strategy was proposed in [37], where the flexible load agents gain their regulation capacities from the dispatch centre through bidding with generating units, but the minimal and maximal capacities of the aggregators are supposed to have the same value for simplicity.

Above all, we can see that the dynamic performance and control strategy are essential research topics when systems are subjected to application[18, 28, 37]. And the main challenge in utilizing air-conditioner clusters for min-level generation following is to achieve precise and reliable control while adapting to load variations over a relatively longer response time period. Previous research has explored various control strategies for load following services, but challenges remain in improving control accuracy[35][36] and ensuring dynamic

response capacities[38][37]. Overall, addressing these challenges is essential for effective application and optimization of air-conditioner clusters in providing min-level generation following services. Hence, this paper designs a self-constraint MPC for the min-level generation following service, which could consider the rehearsed temporal knowledge while finishing the tracking task. The contributions of this paper are summarized as follows:

1) A self-constraint MPC for the min-level generation following service is designed in this paper, which aims at utilizing the tracking ability of aggregated ACCs by considering the rehearsed knowledge of the specific ACCs, thus achieving a more reliable response effect. The proposed self-constraint MPC consists of three main parts: response rehearsal, distributed consistency based power allocation and real-time task execution.

2) Among the self-constraint MPC, the rehearsal knowledge of each cluster is examined by a rehearsal MPC, where the prior factors, the upward/downward limits $[L_{\mathrm{i}}, U_i]$ and control cost function $\phi\left(P_{\mathrm{rmpc}}\right)$ could be obtained; on this basis, the coherence of the incremental response costs of different clusters are achieved by containing the prior factors to model the constraints and cost functions. The schematic framework of self-constraint MPC for min-level generation following is illustrated in Fig.1.

3) To be suitable for the application, a novel state space model for the aggregate power of ACCs is established. To improve the accuracy of the proposed model and capture more of the dynamic fluctuations of the aggregate power, a mixed difference scheme based on the up-wind scheme and Beam-warming scheme are adopted to handle the coupled PDE model.

The organisation of this paper is as follows: Section 2 presents the aggregate state space model of ACCs. Section 3 proposes self-constraint MPC of ACCs for min-level generation following. Section 4 verifies the effectiveness of proposed method under different scenarios. Section 5 discusses the effectiveness of the rehearsed knowledge on the performance self-constraint MPC. And Section 6 gives the conclusion.

2. Air Conditioner Clusters Aggregated Power Modeling

Under the min-level generation following situation, the dynamic fluctuation could not be ignored, to capture the fluctuation process, a state space model based on mixed upwind scheme and Beam-Warming scheme of coupled PDE model is proposed in this section.

2.1. Primary coupled PDE model

In the coupled PDE model, the state evolution of aggregated ACC could be regarded as the fluid along on the temperature axis. When the temperature setpoint is set to T_{set}, the flowing range on the axis, which is also called temperature deadband, is limited to $[T_{\mathrm{set}} - \delta/2, T_{\mathrm{set}} + \delta/2]$. The ACCs flux $L^{\mathrm{ON/OFF}}(t,T)$ going through temperature T (°C) at time t is represented as (1).

$$L^{\mathrm{ON/OFF}}(t,T) = a^{\mathrm{ON/OFF}} N^{\mathrm{ON/OFF}}(t,T) \tag{1}$$

where N^{ONOFF} is the load number at time t on temperature T, a^{ONOFF} is the flowing rate on the temperature range. $a^{\mathrm{ON/OFF}}$ is often regarded as a content, which is represented as: $\bar{a}_{\mathrm{on}} = (T_a - T_{\mathrm{set}} - QR)/CR; \bar{a}_{\mathrm{off}} = (T_a - T_{\mathrm{set}})/CR$, where T_a is the outdoor temperature, C (kWh/°C) is the thermal capacitance and R (°C/kW) is the thermal resistance, Q(kW) is ACC's rated cooling power.

The dynamic evolution of ACs on the temperature range is expressed by the following coupled PDE system:

$$\begin{cases} N_t^{\mathrm{OFF}}(t,T) + \bar{a}_{\mathrm{off}} N_T^{\mathrm{OFF}}(t,T) = 0 \\ N_t^{\mathrm{ON}}(t,T) + \bar{a}_{\mathrm{on}} N_T^{\mathrm{ON}}(t,T) = 0 \end{cases} \tag{2}$$

The flowing rate at the boundary of temperature range is:

$$L_T^{\mathrm{ON}}\left(t, T_{\mathrm{lowhigh}}\right) + L_T^{\mathrm{OFF}}\left(t, T_{\mathrm{low/high}}\right) = 0 \tag{3}$$

where T_{low} and T_{high} are the lower boundary and upper boundary respectively, i.e., $T_{\mathrm{low}} = T_{\mathrm{set}} - \delta/2, T_{\mathrm{high}} = T_{\mathrm{set}} + \delta/2$.

Then the aggregated power P_{sum} (kW) equals to the power consumed by the ACs running at ON state at time t, which is:

$$P_{\mathrm{sum}}(t) = \frac{Q}{\eta} \int_{T_{\mathrm{low}}}^{T_{\mathrm{high}}} N_{\mathrm{on}}(t,T) dT \tag{4}$$

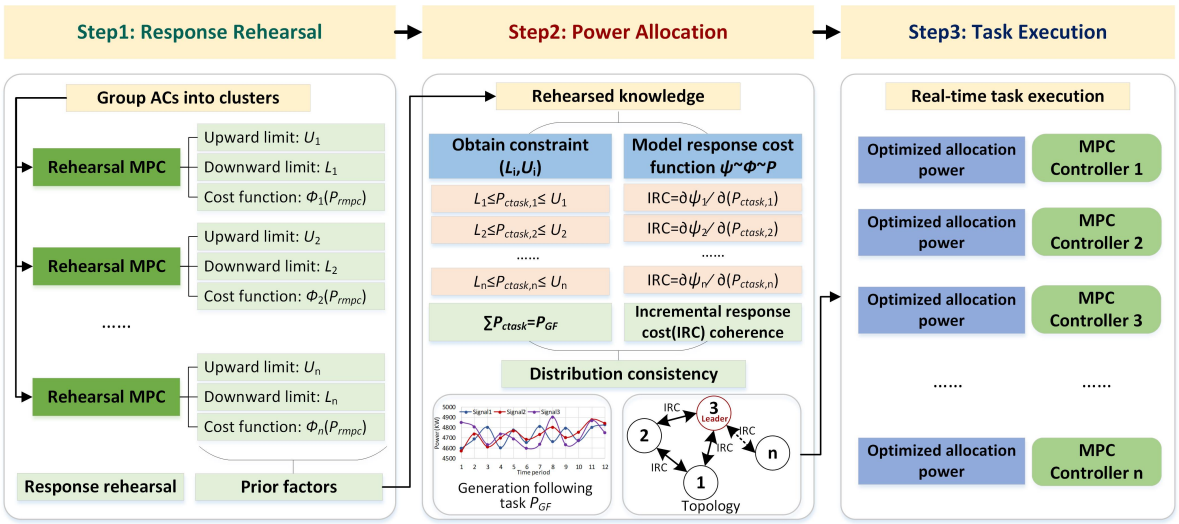

Figure 1: The schematic framework of self-constraint MPC for min-level generation following

2.2. A novel state space model of ACC

To improve the computational accuracy, the classical upwind scheme and Beam-Warming scheme are combined to handle the ACC PDE equations. The schematic diagram of the proposed novel state space(NSS) model is shown in Fig.2. Taking the j^{th} segment at OFF state as an example, the incremental load number $\Delta x_j(k)$ at the sample time k is not only related to the adjacent $j-1^{\text{th}}$ segment, but also the sub-adjacent $j-2^{\text{th}}$ segment. These two increment load sources are represented in Fig.2 in short bule arrows and long curve arrows respectively.

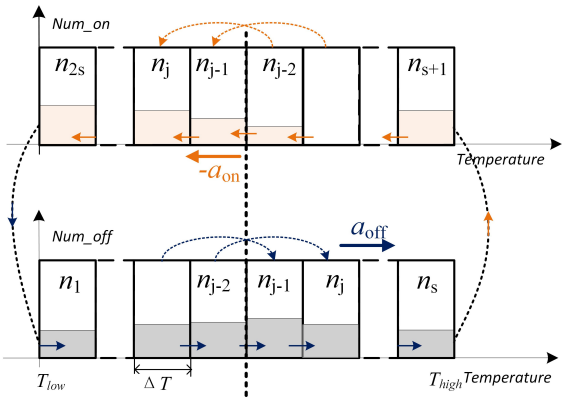

Figure 2: The schematic diagram of NSS model

Due to the coupling between the evolution processes of the off and on states at the boundaries, a first-order differential method from the original model is retained for the boundary and sub-boundary cells to ensure computational stability. The calculation of load increments within temperature cell j using the second-order upwind scheme is given by Eq. (5). For simplicity, the discrete time index k is omitted in the following text, and Δx_j denotes $\Delta x_j(k)$.

$$\Delta x_j = \begin{cases} a_{\text{off}}\lambda(x_{j-1}-x_j) - \frac{a_{\text{off}}\lambda}{2}(1-a_{\text{off}}\lambda)(x_j - 2x_{j-1} + x_{j-2}), \\ \qquad\qquad j = 3,4,\ldots,s \\ a_{\text{on}}\lambda(x_j - x_{j-1}) - \frac{a_{\text{on}}\lambda}{2}(1-a_{\text{on}}\lambda)(x_j - 2x_{j-1} + x_{j-2}), \\ \qquad\qquad j = s+3, s+4,\ldots,2s \end{cases} \tag{5}$$

Here, $j = 3,4,\ldots,s$ represents the temperature cells in the off state, and $j = s+3, s+4,\ldots,2s$ represents the temperature cells in the on state. λ denotes the ratio of the sampling time to the width of the temperature cell, i.e., $\lambda = \Delta t/\Delta\theta$.

For the sub-boundary cells Δx_j (where $j = 2$ and $j = s+2$), if calculated using Equation (5), the temperature will exceed the temperature state space $[T_{\min}, T_{\max}]$. Therefore, Equation (6) and (7) are used for these cases.

$$\Delta x_2 = a_{\text{off}}\lambda(x_1 - x_2) \tag{6}$$

$$\Delta x_{s+2} = a_{\text{on}}\lambda(x_{s+2} - x_{s+1}) \tag{7}$$

For the boundary cells, the calculation method is given by Equation (8).

$$\Delta x_1 = -a_{\text{off}}x_1\lambda - a_{\text{ob}}x_{2s}\lambda \tag{8}$$

$$\Delta x_{s+1} = a_{\text{on}}x_{s+1}\lambda + a_{\text{off}}x_1\lambda \tag{9}$$

The aggregated power of the AC cluster is given by:

$$P_{\text{agg}} = \frac{Q}{\eta}\sum_{j=s}^{2s} x_j \tag{10}$$

The above discrete expressions can be formulated into matrix expressions as:

$$\begin{cases} \boldsymbol{x}(k+1) = \boldsymbol{x}(k) + \Delta\boldsymbol{x}(k) = (\boldsymbol{I} + \Delta t \cdot \boldsymbol{O})\,\boldsymbol{x}(k) \\ y(k+1) = \boldsymbol{C}x(k+1) \end{cases} \tag{11}$$

2.3. Verification

The accuracy of the proposed NSS model is compared with the primary state space model and Monte-Carlo method. The parameters of ACC [39] are shown in Table.1.

Table 1: Parameters of air conditioner cluster

Parameter	Mean	Standard Deviation
$C/$ (kWh/°C)	0.2	0.02
$R/$ (°C/kW)	5.9	0.06
$Q/$(kW)	3.0	0.30
η	3.0	0.30
Tout	34.0	0.34

In the simulation, the initial distribution of ACC are set as the same. The proposed NSS model is compared with the classic Monte-Carlo method and also the primary state space model used in Ref.[39]. The evolution of aggregated power is shown in Fig.3. It can be observed that the final stable aggregated power of the three models trend to be the same, but there is obvious bias during the fluctuation stage. And the proposed model performs better when describing the fluctuation stage power.

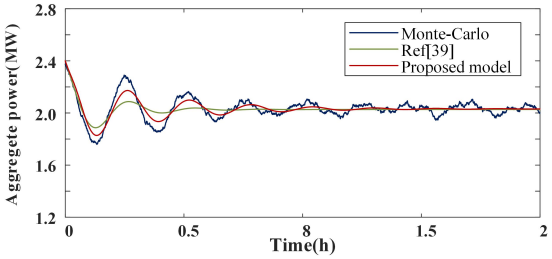

Figure 3: Accuracy verification of proposed high-accuracy model[39]

3. Self-constraint MPC of ACCs for min-level Generation Following

According to the state evolution law of ACCs[34], the single AC device belonging to a cluster could be seen as a particle that follows a stochastic behaviour[40]. This means that if no forced control actions are given to the ACCs, the aggregate power will recover to a stable value after certain iterations at an arbitrary initial load distribution, as shown in Fig.3. This characteristic implies that the response potential of air conditioner clusters is not infinite. Previous research has indicated that for a specific ACC, a higher adjustment ratio of aggregated power leads to a shorter response duration,as seen in Fig.4. The unreasonable allocated task assigned to the ACC may prevent the ACs from accurately tracking the reference signal within the required response period.

To address this issue, this section proposes an self-constraint MPC to consider the temporal response knowledge of specific ACCs. Firstly, the temporal response knowledge is obtained by rehearsal MPC, and then the distribution consistency based task allocation method is designed on the basis of the prior factors obtained by the previous stage. Lastly, the real-time MPC is used for the task execution.

3.1. Rehearsal MPC

To obtain the temporal response limitation of a specific ACC, we first categorize the heterogeneous air conditioners into several clusters by their running state. According to the previous research, the power baseline of an ACC is directly influenced by the temperature setpoint, hence, the whole AC population is considered as a multi-agent system. Each agent would undertake parts of the generation following task.

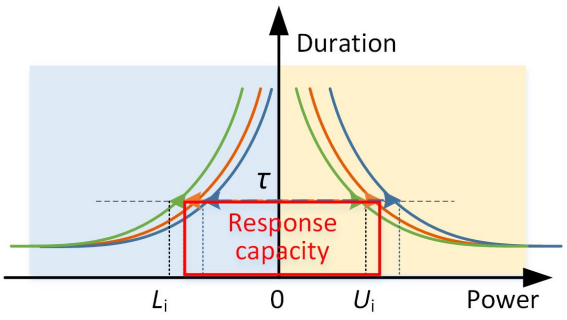

Figure 4: The mechanism of proposed methodology

3.1.1. $[L_i, U_i]$ searching

Considering that the function of the response limitation is not explicit, the performance of the ACC is evaluated by the self-constraint MPC process, to obtain the approximate expression. For the ACC agent, the optimization control objectives and constraints of MPC are shown in (12).

$$\begin{aligned} &\min F = \left(\boldsymbol{y}(k) - \boldsymbol{P}_{\text{rmpc}}\right)^T \boldsymbol{Q}\left(\boldsymbol{y}(k) - \boldsymbol{P}_{\text{rmpc}}\right) + \boldsymbol{u}(k)^T \boldsymbol{R}\boldsymbol{u}(k) \\ &\text{s.t.} \begin{cases} \boldsymbol{x}(k) = (\boldsymbol{I} + \boldsymbol{O})\boldsymbol{x}(k-1) + \boldsymbol{B}\boldsymbol{u}(k) \\ y(k) = \boldsymbol{C}\boldsymbol{x}(k) \\ |\boldsymbol{u}(k)|_{s\times 1} \le \boldsymbol{x}(k-1)|_{(1:s)\times 1} \\ \boldsymbol{x}(k) \ge 0 \end{cases} \quad \forall k = 1, 2, \cdots, n \end{aligned} \tag{12}$$

where F is the objective function; $\boldsymbol{Q}$ is a constant coefficient that representing the tracking error weight; $\boldsymbol{R}$ is the penalty weight coefficient matrix of the control variable, which only contains non-zero elements at diagonal. $\boldsymbol{y(k)}$ is the predicted aggregate power of ACC; $\boldsymbol{u}(k)$ is the control variable that indicates the operating states switching of air conditioners within the temperature state space.

When searching for the upward response limitation, gradually increase the adjustment power $\Delta P_i = k_{\mathrm{f}} * P_{\mathrm{base},i}$ of ACC at a time, record the number of controller actions $\phi(P_{\mathrm{test}})$. When the error between the output power $\boldsymbol{y}(k)$ and the target power $\boldsymbol{P}_{\mathrm{rmpc}}$ exceeds the acceptable control bias, the searching would be stopped. The stop boundary would be recorded as the response adjustment boundary of specific ACC. SImilarly, the downward response limiation could also be obtained. The proposed algorithm is elaborated as follows:

Algorithm 1 Response rehearsal algorithm

1: Calculate $P_{\mathrm{base},i}$ of each ACC, $P_{\mathrm{base},i} \approx N_{\mathrm{sum},i}\left(T_a - T_{\mathrm{set},i}\right)/\eta R$.
2: Initialize the adjustment power step $\Delta P_i = k_{\mathrm{f}} * P_{\mathrm{base},i}$, the rehesersal duration τ
3: Searching for the upward response limitation
4: **while** stopping condition is not triggered **do**
5: Repeat the rehearsal MPC in (12),
6: Record the control actions number under the corresponding tracking power P_{rmpc}
7: If the tracking error is acceptable, $P^{i+1}_{\mathrm{rmpc}} = P^{i}_{\mathrm{rmpc}} + \Delta P_i$, else record P_{rmpc} as U_i
8: **end while**
9: Searching for the downward response limitation
10: **while** stopping condition is not triggered **do**
11: Repeat the rehearsal MPC in (12),
12: Record the control actions number under the corresponding tracking power P_{rmpc}
13: If the tracking error is acceptable, $P^{i+1}_{\mathrm{rmpc}} = P^{i}_{\mathrm{rmpc}} - \Delta P_i$, else record P_{rmpc} as L_i
14: **end while**
15: **Output:** the limits of ACCs $[L_{\mathrm{i}}, U_i]$, and mapping $\phi\left(P_{\mathrm{rmpc}}\right)$

3.1.2. $\psi(P_{ctask})$ modeling

Besides, the relationship between the number of controller actions $\phi(P_{\mathrm{test}})$ and the test power $\boldsymbol{P}_{\mathrm{rmpc}}$ would be fitted into a quadratic function. Repeat the aforementioned method to evaluate the downward response limitation. Thus, the response limitation of ACC through the self-constraint could be represented as:

$$\begin{aligned}\phi\left(P_{\mathrm{rmpc}}\right) =& \rho_i\left(P_{\mathrm{rmpc}} - P_{\mathrm{base}}\right)^2 + \epsilon_i\left(P_{\mathrm{rmpc}} - P_{\mathrm{base}}\right), \\ & P_{\mathrm{rmpc}} \in [L_i, U_i]\end{aligned} \tag{13}$$

where P_{base} is the baseline aggregated power of a specific ACC under the stable state. ρ_i and ϵ_i can be fitted according to the self-constraint MPC results. It worth be noting that a implicit information of expression (13) is that when the tracking power signal is closer to P_{base}, the smaller the switching number in the ACC cluster will be, which is reasonable.

We define the response cost function to represent the cost for ACC operators when participating in the slow-generation following service, which could be modelled as:

$$\psi\left(P_{\mathrm{rmpc}}\right) = k_c \cdot \phi\left(P_{\mathrm{rmpc}}\right) + k_a \cdot N_{\mathrm{sum}} \tag{14}$$

where ϕ is the total switching number during the response for the i^{th} ACC. kc_i is the control cost that happens every control for the i^{th} ACC, which is 0.02\$/ switch in this paper, ka_i is the one-time subsidies given to the customer for the i^{th} ACC, which is assumed as 0.1\$ per AC.

By integrating (13) and (14), the control cost function can be derived in (15).

$$\begin{aligned}&\psi_i\left(P_{\mathrm{rmpc},i}\right) = \alpha P^2_{\mathrm{rmpc},i} + \beta P_{\mathrm{rmpc},i} + \gamma \\ &\begin{cases}\alpha = kc_i \cdot \rho_i \\ \beta = kc_i \cdot \epsilon_i - 2kc_i \cdot \rho_i P_{\mathrm{base},i} \\ \gamma = kc_i \cdot \rho_i P^2_{\mathrm{base},i} - kc_i \cdot \epsilon_i P_{\mathrm{base},i} + ka_i \cdot N_i\end{cases}\end{aligned} \tag{15}$$

3.2. Rehearsed knowledge-based power allocation

The distributed control framework is adopted in this paper, which could ensure the response reliability as much as possible in case of unpredictable dropouts due to certain communication failures or other types of uncertainty. The coherence of different clusters under the distribution control paradigm is achieved by the virtual regulation cost, which contains both the control cost and the control limitation simultaneously. The total power tracking signal is given to the leader ACC, and the leader ACC exchanges the power the power allocation algorithm converges to the optimal result, the power tracking instructions are then performed by real-time MPC controller.

This power allocation strategy aims to minimize the regulation cost of all the agents within the load aggregator under the condition of satisfying the operating constraints of each ACC. The mathematical model can be

written as:

$$\begin{aligned} &\min \Theta = \sum_{i \in G_{LA}} \psi_i \left(P_{\text{ctask},i}\right) \\ &\text{s.t.} \left\{ \begin{array}{l} P_{\text{GF}} = \sum_{i \in S_{LA}} \left(P_{\text{ctask},i}\right) \\ L_i P_{\text{base},i} \leq P_{\text{task},i} \leq U_i P_{\text{base},i} \end{array} \right. \end{aligned} \tag{16}$$

where i is the number of ACCs. The equality constraint in (16) ensures the total reference power P_{GF} can be tracked by all the agents. L_i and U_i are respectively the lower and upper aggregate power limits of ACC i, which can also be obtained by the method proposed in subsection 3.1.

Let ζ denotes the Lagrange multiplier corresponding to the equation constraint, the equation constraint optimization problem can be translated into (17).

$$\min \Theta = \sum_{i \in G_{LA}} \psi_i \left(P_{\text{ctask},i}\right) + \zeta \left(P_{\text{GF}} - \sum_{i \in G_{LA}} P_{\text{ctask},i} \right) \tag{17}$$

The equation (18) is obtained by the partial derivative for $P_{\text{ctask},i}$, which means that the optimal solution to the power allocation problem is to make the incremental reponse cost (IRC) of each ACC equal to each other. m is the number of agents in the LA.

$$\frac{\partial \psi_1}{\partial P_{\text{ctask},1}} = \frac{\partial \psi_2}{\partial P_{\text{ctask},2}} = \cdots = \frac{\partial \psi_m}{\partial P_{\text{ctask},m}} = \zeta \tag{18}$$

Select IRC as the consensus variable, and the IRC update formula of Follower agent is:

$$\zeta_i(k+1) = \sum_{l=1}^{n} a_{il} \zeta_l(k) \quad i \in G_{\text{LA}} \tag{19}$$

In order to ensure that the total aggregate power of all agents is balanced with the following command, the bias between the actual total allocated power and reference power P_{GF} is represented by ΔP :

$$\Delta P = P_{\text{GF}} - \sum_{i \in G_{LA}} P_{\text{ctask},i} \tag{20}$$

The leader agent can be chosen by central retrieval. Leader agent's IRC update formula is as follows:

$$\zeta_i(k+1) = \sum_{l=1}^{n} a_{il} \zeta_f(k) + \mu \Delta P \quad i \in G_{\text{LA}} \tag{21}$$

where the μ is a positive convergence coefficient.

Equation (22) can be obtained by (18) and (20):

$$P_{\text{ctask},i} = \frac{\zeta_i - \beta_i}{2\alpha_i}, i \in G_{\text{LA}} \tag{22}$$

The power constraint of the ACC can be modified as:

$$P_{\text{ctask},i} = \left\{ \begin{array}{ll} L_i P_{\text{ctask},i}, & P_{\text{ctask},i} < \zeta_{i,\,\min} \\ \left(\zeta_i - \beta_i\right)/2\alpha_i, & P_{\text{ctask},i} \in \left[L_i P_{\text{base},i}, U_i P_{\text{base},i}\right] \\ U_i P_{\text{ctask},i}, & P_{\text{ctask},i} > \zeta_{i,\max} \end{array} \right. \tag{23}$$

3.3. MPC real-time control

After deriving the optimized allocation power, the controller of each ACC agent would execute the MPC optimization formula given in (12), respectively.

4. Case Study

To verify the effectiveness of the proposed self-constraint MPC framework of ACCs for min-level generation following service. This section presents the simulation details of the proposed method. The GF signal issued by the corresponding renewable power generation transactor is 5 min at intervals and lasts for 1h, as shown in Fig.5.(a). Suppose that there are 12000 air conditioners belonging to one local load aggregator, all the ACs are categorized by their temperature set-points, and they are numbered as C1, C2, $\cdots$, C5, respectively. In this section, Signal 1 is adopted to verify the effectiveness of SMPC and presents the details of the execution details. The superiority of the proposed response strategy would be verified through different generation following signals in Section5. The communication topology is as shown in Fig.5.(b).

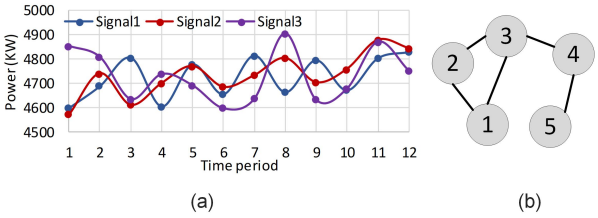

Figure 5: Given information: generation following signal and topology

4.1. Step1: Response rehearsal simulation of ACCs

Tab.2 is the prior factors obtained by the response rehearsal. L_{i} and U_i describing the response limitation of the ACCs are derived. α, β, γ are the coefficients of the cost function, respectively. It could be seen that the both the lower response limitations L_{i} and upper response limitations U_{i} of ACCs would increase as the increasing of temperature setpoints. And the length of the limits range $[L_{\text{i}}, U_{\text{i}}]$ varies between (0.7,1.0) for the given τ. This rehearsed knowledge provides a reference for the application of utilizing ACCs providing the ancillary services.

Table 2: Prior factors by response rehearsal

#	T_{set}	$[L_i, U_i]$	α	β	γ	P_{base} (kW)
C1	24	[0.56, 1.25]	0.00079	-0.8035	304.31	506.7
C2	25	[0.60, 1.35]	0.00019	-0.5248	654.87	1351.0
C3	26	[0.63, 1.45]	0.00013	-0.4047	719.89	1575.6
C4	27	[0.75, 1.50]	0.00017	-0.3454	477.50	1012.4
C5	28	[0.80, 1.80]	0.00071	-0.4058	157.64	281.0

4.2. Step2: Distributed power allocation verification

Fig.6 shows the converged process of ΔP for all the 12 time periods during the whole response period under the generation following signal 1. It can be found that the distributed power allocation algorithm will converge within 1s, which can meet the time requirement of online power allocation optimization.

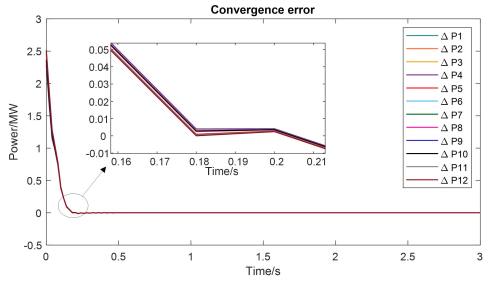

Figure 6: Converged process of ΔP at each power tracking point

Besides, Fig.7 depicts the dynamic converged process of IRC (seen as Fig.7 (a)-(e)) and the final values after the algorithm is converged (seen as Fig.7 (f)) of the ACCs. It could be seen that for all the 12 time periods, the consensus variables IRC of different time periods would converged to different values. As depicted in Fig.7 (f), the converged IRC values at different time periods vary between $-0.015 \sim 0.007$\$/kW, for the 1^{st}, 2^{nd}, 4^{th}, 6^{th}, 8^{th} and 10^{th} time periods, the IRC will converge to a negative value. This is because the tracking power of these periods are below the power baseline of all the agents. The negative IRC means that if the allocated power is increased, the aggregate power would be closer to the baseline, then response cost would decrease correspondingly. When the tracking power is above the power baseline for the other remaining time periods, the IRC would converged to a positive value, as versa. More specifically, we could find that the converged process of different ACCs are different. Among the five ACC agents, the convergence speed of ACC3 is much quicker than other follower agents. This is because the ACC3 is chosen as the leader agent, and the convergence error of the aggregate power of all the clusters and the tracking power would be firstly perceived by

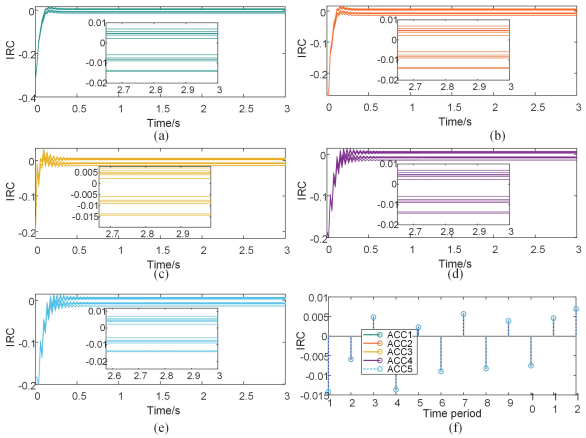

Figure 7: Converged process of IRC at each power tracking point

the leader agents, and the follower agents would change their aggregate power accordingly.

4.3. Step3: Task execution results comparison

To verify the effectiveness the distribution consistency-based control strategy proposed in this article, two allocation methods are compared in the simulation: 1) Equal proportional MPC strategy (EMPC): the generation following signal is sent proportional to the power baseline of ACs in each agent. 2) Self-constraint MPC strategy.

The time resolution of MPC controller is set as 3s, which means that 100 steps will be executed during each 5 min. The weight coefficient matrix $\boldsymbol{R}$ is set as diag[0.1 0.3 0.5 0.7 0.9 0.9 0.7 0.5 0.3 0.1]. This non-uniform coefficient matrix is set to consider the different response potential of ACC at different temperature cells.

The task execution results by EMPC strategy and SMPC strategy are presented in Fig.8.The specific outputs of ACC1- ACC5 are exhibited in Fig.8.(a)-(e), respectively. It can be seen that although the deviation of the following power task allocated to ACCs by these two strategies is not large, the final execution result of SMPC shows a better performance. Especially, the large tracking error of ACC1, as shown in Fig.8.(a), embodies the significance and necessity of reasonable power

allocation when participating the min-level generation following signal.

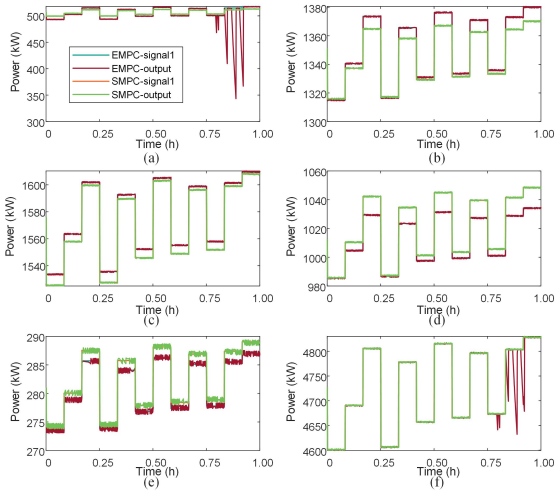

Figure 8: EMPC and SMPC execution results for Signal 1, (a)-(e) ACC1-ACC5,(f) total output

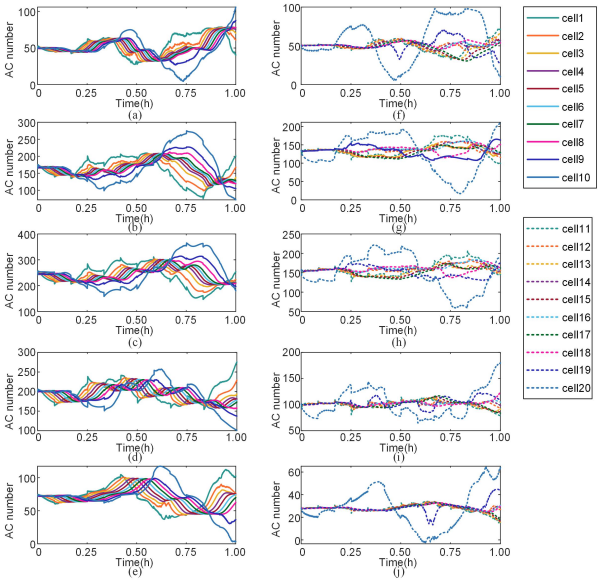

Figure 9: ACC number behaviours during response

Furthermore, Fig.9 shows the entire details of the ACCs, where the subplots Fig.9(a)-(e) represent the state variables running at the off-state, and the subplots Fig.9(f)-(j) represent the on-state ACCs. It can be seen that during the response time period from 0h to 0.08h, the AC number in cells11 to cells20 are all decrease obviously, which means that the ACs at the on state are forced into off state. However, the AC number in cell10 keeps a relative stable value, seen as Fig.9(a)-(e), due to the natural temperature raises when ACs are running at the off state, and the results are corresponding with the details of control variables.

5. Discussion

To discuss the availability of the proposed SMPC strategy, different generation following signals are firstly tested in this section. Then, the effectiveness of the response limits are also verified.

5.1. Response performance verification: Signal 2 and Signal 3

The min-level generation following Signal 2 in Fig. 5 exhibits a fluctuating upward trend during the response window, and Signal 3 corresponds to a scenario with a larger mean squared error for the signal. The converged IRC and execution results under these two signals are presented in Fig. 10 and Fig. 11, respectively. It is evident that the SMPC performs well for both signals, and the converged IRC reflects the shape of the following signal to some extent. Additionally, when tracking the upward trending Signal 2, there is a slight spike during ACC5 tracking the task, but it quickly recovers and achieves accurate tracking.

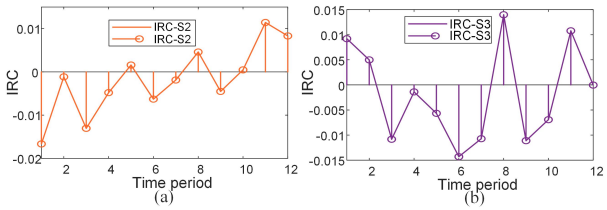

Figure 10: Converged IRC under three signals

5.2. Upward/downward limits effectiveness verification

To investigate the influence of response limits L_i and U_i on power allocation and task execution, the limit ranges of each cluster in the distribution power allocation are changed to new ranges, referred to as "test limit range" in this subsection. The specific details are presented in Fig. 12. The limits of ACC1, ACC3 and ACC5 are kept the same as the previous limit range to ensure the total available power for the generation following service, To verify the effectiveness of the limits, the limit range of ACC2 is set to a lower zone, indicating that the entire population in ACC2 would undertake a downward power task. In contrast, ACC4 is assigned

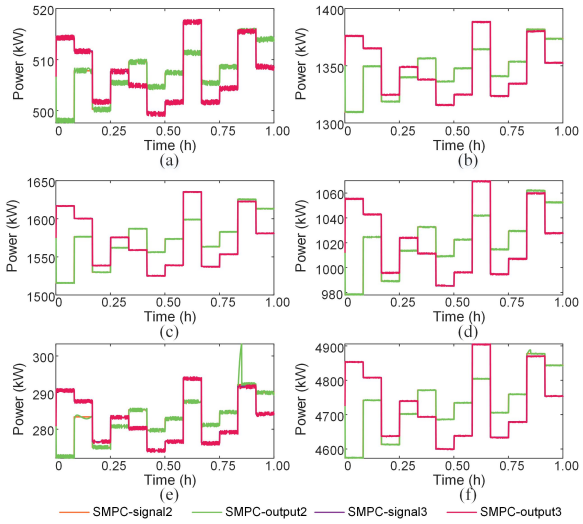

Figure 11: Execution results,where (a)-(e) are the outputs of ACC1-ACC5 and (f) is the total output

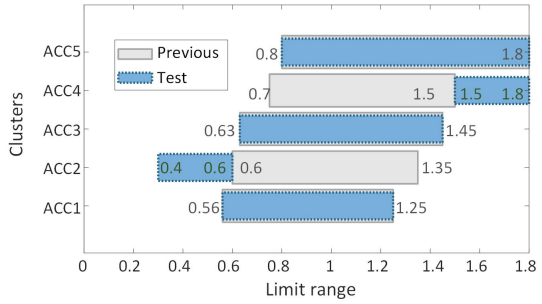

Figure 12: Convergence process of Δ P at each period

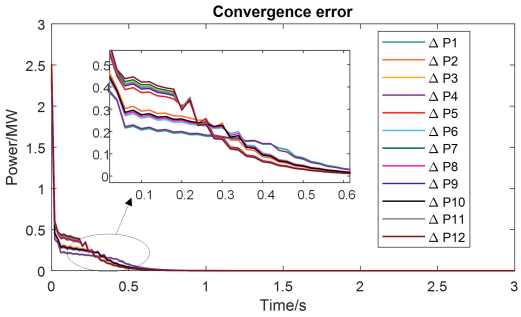

Figure 13: Convergence process of Δ P at each period

with a higher limit range compared with the previous range.

Under the test limit range scenario, Fig. 13 illustrates the convergence process of the power bias ΔP. The power allocation algorithm reaches convergence at approximately $t = 0.7$ seconds, which is comparatively slower than the previous limit range scenario. Additionally, Fig. 14 presents the converged IRC of each cluster. Similar to the previous scenario, the IRC of different clusters converges to equal values for each specific time period. However, in this test limit range scenario, the values are larger. Fig. 15 further shows the outputs of the MPC in the task execution stage. There is an evident tracking error, even though the allocation converges. The slower convergence of the power allocation algorithm and the presence of tracking errors in Fig. 15 suggest that the test limit range scenario impacts both the speed of convergence and the overall accuracy of the power allocation.

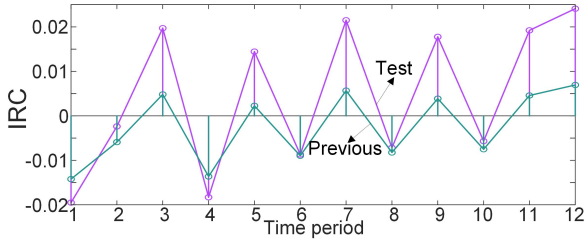

Figure 14: Converged IRC of each ACC

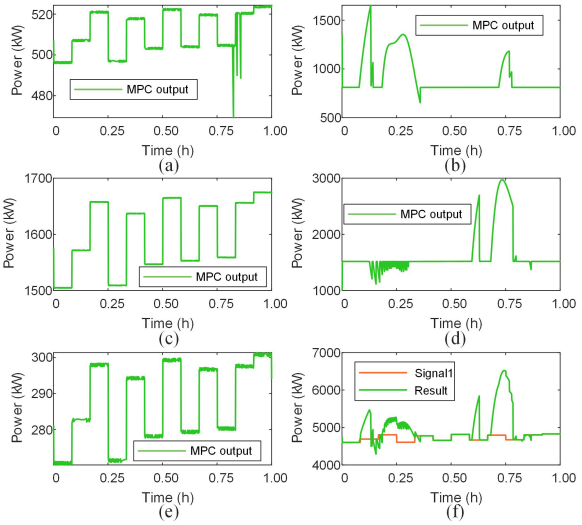

Figure 15: MPC outputs under the test limit range scenario

6. CONCIUSION

In this paper, a self-constraint MPC for the min-level generation following service is proposed, which could consider the rehearsed temporal response limitations and the response costs while allocating the following task to different clusters. The conclusions of this paper are summarized as follows:

1)Through the response rehearsal MPC for evaluation the prior knowledge of different air conditioner clusters, it could be found that both the lower response limitations L_{i} and upper response limitations U_{i} of ACCs would increase as the increasing of temperature setpoints. This rehearsed knowledge provides a reference for the application of utilizing ACCs providing the ancillary services.

2)Under different generation following signals, the proposed self-constraint MPC could perform well, and the converged IRC reflects the shape of the following signal to some extent. Besides, the effectiveness of the limit range obtained by the response rehearsal is verified by simulation. And the results show that if the limits range are set when not considering the prior knowledge, the power allocation algorithm may still converge to a reasonable value, but the real-time task execution may experience large tracking errors.

References

[1] Climate Change - What You Need to Know, 2023. https://www.un.org/climatechange?gclid=CjwKCAjw-7OlBhB8EiwAnoOEkySRjIYb390vsJYA_PjCfXOLLruyZx9MXhgRs7IAleV-J38alLSfmBoCq5oQAvD_BwE.

[2] Net Zero by 2050 – Analysis - IEA, Technical Report, 2021.

[3] S. Fankhauser, S. M. Smith, M. Allen, K. Axelsson, T. Hale, C. Hepburn, J. M. Kendall, R. Khosla, J. Lezaun, E. Mitchell-Larson, et al., The meaning of net zero and how to get it right, Nature Climate Change 12 (2022) 15–21.

[4] S. Dale, https://www.bp.com/content/dam/bp/business-sites/en/global/corporate/pdfs/energy-economics/energy-outlook/bp-energy-outlook-2023.pdf, Technical Report, BP, 2023.

[5] Energy transition trends 2023, 2023. https://www.spglobal.com/commodityinsights/PlattsContent/_assets/_files/en/specialreports/energy-transition/10-cleantech-trends-in-2023.html.

[6] S. Impram, S. V. Nese, B. Oral, Challenges of renewable energy penetration on power system flexibility: A survey, Energy Strategy Reviews 31 (2020) 100539.

[7] Y. Li, M. Han, M. Shahidehpour, J. Li, C. Long, Data-driven distributionally robust scheduling of community integrated energy systems with uncertain renewable generations considering integrated demand response, Applied Energy 335 (2023) 120749.

[8] S. Rusche, J. Weissflog, S. Wenninger, B. Häckel, How flexible are energy flexibilities? developing a flexibility score for revenue and risk analysis in industrial demand-side management, Applied Energy 345 (2023) 121351.

[9] N. A. E. R. C. I. W. Group, et al., Defining interconnected operations services under open access: Final report, NERC, March (1997).

[10] E. Hirst, B. Kirby, Unbundling generation and transmission services for competitive electricity markets: examining ancillary services, Oak Ridge National Laboratory, 1998.

[11] E. Hirst, B. Kirby, Separating and measuring the regulation and load-following ancillary services, Utilities Policy 8 (1999) 75–81.

[12] Lfas market participation, https://aemo.com.au/energy-systems/electricity/wholesale-electricity-market-wem/participate-in-the-market/information-for-current-participants/lfas-market-participation, 2022.

[13] Increasing the penetration of renewable energy sources in the distribution grid by developing control strategies and using ancillary services, 2013. https://cordis.europa.eu/project/id/608998.

[14] E. Nobile, A. Bose, K. Tomsovic, Feasibility of a bilateral market for load following, IEEE Transactions on Power systems 16 (2001) 782–787.

[15] E. De Tuglie, F. Torelli, Load following control schemes for deregulated energy markets, IEEE Transactions on Power systems 21 (2006) 1691–1698.

[16] R. J. Abraham, D. Das, A. Patra, Load following in a bilateral market with local controllers, International Journal of Electrical Power & Energy Systems 33 (2011) 1648–1657.

[17] S. Li, K. Tomsovic, T. Hiyama, Load following functions using distributed energy resources, in: 2000 Power Engineering Society Summer Meeting (Cat. No. 00CH37134), volume 3, IEEE, 2000, pp. 1756–1761.

[18] W. Yao, K. Y. Lee, A control configuration of wind farm for load-following and frequency support by considering the inertia issue, in: 2011 IEEE Power and Energy Society General Meeting, 2011, pp. 1–6. doi:10.1109/PES.2011.6039511.

[19] H. Fakham, D. Lu, B. Francois, Power control design of a battery charger in a hybrid active pv generator for load-following applications, IEEE Transactions on Industrial Electronics 58 (2010) 85–94.

[20] A. Lokhov, Load-following with nuclear power plants, NEA news 29 (2011) 18–20.

[21] R. Loisel, V. Alexeeva, A. Zucker, D. Shropshire, Load-following with nuclear power: Market effects and welfare implications, Progress in Nuclear Energy 109 (2018) 280–292.

[22] E. R. EC, Energy roadmap 2050, COM/2011/0885 (2011).

[23] Y. Zhu, K. Tomsovic, Development of models for analyzing the load-following performance of microturbines and fuel cells, Electric Power Systems Research 62 (2002) 1–11.

[24] P. Mago, L. Chamra, J. Ramsay, Micro-combined cooling, heating and power systems hybrid electric-thermal load following operation, Applied Thermal Engineering 30 (2010) 800–806.

[25] A. Cagnano, E. E. De Tuglie, R. Turri, F. Bignucolo, Microturbine control strategy for the load-following service provision, in: 2020 AEIT International Annual Conference (AEIT), 2020, pp. 1–5. doi:10.23919/AEIT50178.2020.9241091.

[26] S. Massucco, A. Morini, G. Petretto, A. Pitto, F. Silvestro, A solid oxide fuel cell model to investigate load following and stability issues in distribution networks, in: 2009 IEEE Bucharest PowerTech, 2009, pp. 1–7. doi:10.1109/PTC.2009.5282267.

[27] N. Bizon, Real-time optimization strategies of fuel cell hybrid power systems based on load-following control: A new strategy, and a comparative study of topologies and fuel economy obtained, Applied Energy 241 (2019) 444–460.

[28] R. Wang, X. Wang, G. Shu, H. Tian, J. Cai, X. Bian, X. Li, Z. Qin, L. Shi, Comparison of different load-following control strategies of a sco2 brayton cycle under full load range, Energy

246 (2022) 123378.
[29] J. Hui, Y.-K. Lee, J. Yuan, Eso-based adaptive event-triggered load following control design for a pressurized water reactor with samarium–promethium dynamics, Energy 271 (2023) 127058.
[30] K. Ma, Y. Dong, S. Liu, H. Wang, J. Yang, D. Zhang, Cost-effective control strategy for thermostatically controlled loads based on tracking differentiator in smart grid, IET Generation, Transmission & Distribution 13 (2019) 5569–5576.
[31] L. Herre, S. Kazemi, L. Söder, Quantifying flexibility of load aggregations: impact of communication constraints on reserve capacity, IET Generation, Transmission & Distribution 14 (2020) 5211–5218.
[32] Y.-Q. Bao, M. Hu, Y.-Y. Hong, P.-P. Chen, J.-Q. Ju, G. Ma, Accuracy analysis and improvement of the state-queuing model for the thermostatically controlled loads, IET Generation, Transmission & Distribution 11 (2017) 1303–1310.
[33] S. A. Saleh, P. Pijnenburg, E. Castillo-Guerra, Load aggregation from generation-follows-load to load-follows-generation: Residential loads, IEEE Transactions on Industry Applications 53 (2017) 833–842. doi:10.1109/TIA.2016.2626261.
[34] D. S. Callaway, Tapping the energy storage potential in electric loads to deliver load following and regulation, with application to wind energy, Energy Conversion and Management 50 (2009) 1389–1400.
[35] N. Lu, An evaluation of the hvac load potential for providing load balancing service, IEEE Transactions on Smart Grid 3 (2012) 1263–1270. doi:10.1109/TSG.2012.2183649.
[36] J. Hu, J. Cao, M. Z. Chen, J. Yu, J. Yao, S. Yang, T. Yong, Load following of multiple heterogeneous tcl aggregators by centralized control, IEEE Transactions on Power Systems 32 (2016) 3157–3167.
[37] J. Hu, J. Cao, T. Yong, J. M. Guerrero, M. Z. Chen, Y. Li, Demand response load following of source and load systems, IEEE Transactions on Control Systems Technology 25 (2016) 1586–1598.
[38] J. Wang, R. Qiu, B. Xu, H. Wu, L. Tang, M. Zhang, M. Ding, Aggregated large-scale air-conditioning load: Modeling and response capability evaluation of virtual generator units, Energy 276 (2023) 127570.
[39] Y. Ma, Z. Mi, R. Zhang, H. Peng, Y. Jia, Hybrid control strategy for air-conditioning loads participating in peak load reduction through wide-range transport model, Journal of Modern Power Systems and Clean Energy 10 (2021) 1542–1551.
[40] R. Malhame, C.-Y. Chong, Electric load model synthesis by diffusion approximation of a high-order hybrid-state stochastic system, IEEE Transactions on Automatic Control 30 (1985) 854–860.